

Ayón–Beato–García black hole coupled with a cloud of strings: thermodynamics, shadows and quasinormal modes

Amit Kumar^{*a}, Dharm Veer Singh^{† ‡a}, and Sudhaker Upadhyay^{§ ¶ †b,c}

^aDepartment Physics, Institute of Applied Science and Humanities, GLA University,
Mathura - 281406, Uttar Pradesh, India

^bDepartment of Physics, K.L.S. College, Nawada, Magadh University, Bodh-Gaya, Nawada
805110, India

^cSchool of Physics, Damghan University, P.O. Box 3671641167, Damghan, Iran

Abstract

We find an exact black hole solution for the Einstein gravity in the presence of Ayón–Beato–García non-linear electrodynamics and a cloud of strings. The resulting black hole solution is singular, and the solution becomes non-singular when gravity is coupled with Ayón–Beato–García non-linear electrodynamics only. This solution interpolates between Ayón–Beato–García black hole, Letelier black hole and Schwarzschild black hole in the absence of cloud of strings parameter, magnetic monopole charge and both of them, respectively. We also discuss the thermal properties of this black hole and find that the solution follows the modified first law of black hole thermodynamics. Furthermore, we estimate the solution’s black hole shadow and quasinormal modes.

Keywords: Black hole solution; Ayón–Beato–García non-linear electrodynamics; Cloud of strings; Thermodynamics; Black hole shadow; Quasinormal modes.

1 Introduction

Black holes (BHs) are one of the fascinating predictions of general relativity. This is one of the solutions of Einstein’s field equation. Several observations were performed to confirm its existence. The existence was first approved when LIGO detected the first gravitational waves from the BH merger [1]. Recently, the Event Horizon Telescope (EHT) detected the shadow of the BH at the centre of Messier 87* galaxy [2]. Recently, EHT observed the shadow of Sagittarius A* BH around the centre of Milky Way [3]. When the bright light comes in the vicinity of a BH, the light bends and is pulled by the intense gravity of the BH, creating a shadow around the BH where no light can reach an observer.

Born and Infeld were the first to introduce non-linear electrodynamics (NLED) to eliminate the central singularity of a point charge and energy divergence [4]. The NLED became more popular when NLED emerged as limiting cases of specific string theory [5]. It is well-known that the linearity of electrodynamics does not hold at high energies because of the influence of other (physical) fields. In these circumstances, NLED theories may be considered a suitable alternative. NLED, as a source of gravity, is capable to create various new BH solutions [6, 7, 8, 9]. Beyond these, NLED theories play an important role in cosmology [10, 11, 12] and string theories [13, 5]. Ayón–Beato–García (ABG) proposed the first BH with an NLED field satisfying the weak energy condition [14]. Later, a new regular exact BH solution was obtained for an NLED coupled to

* ammiphy007@gmail.com

† veerdsingh@gmail.com

‡ Visiting Associate, IUCAA, Pune, India

§ sudhakerupadhyay@gmail.com

¶ Corresponding author

† Visiting Associate at IUCAA Pune, India

Einstein's gravity [15]. Further, the magnetic stable BH solution to Einstein equations coupled to ABG NLED was proposed [16]. In 2005, four parametric regular BH solutions were studied for the Einstein equations coupled to ABG NLED [17] and other regular BH solutions are given in [18, 19, 20, 21, 22, 23, 24].

Letelier [25] first proposed the cloud of strings (CS), a model for a pressure-less perfect fluid. Being a model for fundamental constituents of the universe, the strings may have essential implications from the astrophysical and cosmological points of view. The CS has been utilised as the possible material source for the Einstein equations and a generalised BH solution were found [26, 27, 28]. Thus, studying space-time geometry in the presence of ABG NLED and CS will be interesting. Precisely, this is the motivation of the present investigation.

The size and shape of the BH shadow may give crucial information regarding the BH parameters like mass, spin and geometry [29, 30, 31, 32, 33]. For instance, a slightly distorted circular shadow of a BH may provide information on the fast rotating rate of BH. The study of the observed shape of the shadow may boost the understanding of both gravity in extreme conditions and BHs. Recently, Shadow of the Reissner-Nordström BH [34], charged massive BTZ BH [35], and BH [36] coupled with NLED have been studied. We know that BH shadow is closely related to the specific complex characteristic frequencies [37] known as quasinormal modes (QNMs) [38]. The QNMs for regular BHs are studied in [39, 40, 41, 42, 43, 44, 45] and QNMs in Eikonal limit in [46, 47]. Shadow and QNMs are studied in [48].

The BH thermodynamics was studied originally by Bekenstein [49, 50] and Hawking [51] by establishing a connection between entropy and the BH horizon area. Further, it is found that the entropy of the BHs is proportional to the area of horizon [52, 53]. The BH thermodynamics has found interest in many ways [54, 55, 56, 57, 58, 59, 60, 61, 62]. For example, the effects of α' corrections on the thermodynamics of a Reissner-Nordström BH is studied [63]. The non-perturbative correction to the Horava-Lifshitz BH thermodynamics is also analysed [64]. Thermal analysis of BH in de Rham-Gabadadze-Tolley massive gravity in Barrow entropy framework has been done recently [65].

In this paper, we derive an exact BH solution for the Einstein gravity in the background of ABG non-linear electrodynamics and a cloud of strings. Interestingly, the resulting BH solution is singular as the regularity due to non-linear electrodynamics is compensated by the cloud of strings. This solution interpolates between ABG BH, Letelier BH and Schwarzschild BH in the absence of magnetic monopole (MM) charge and both of them, respectively. We explore the horizon structure of the obtained BH solution. We also discuss the thermal properties of this BH solution and find that this follows the modified first law of BH thermodynamics. Furthermore, we discuss the BH shadow and quasinormal modes.

The paper is outlined in the following manner. We deduce a new BH solution for the Einstein gravity in the background of the ABG NLED and CS in Sec. 2. In Sec. 3, we calculate the thermodynamics of the resulting BH solution and find that this follows a modified first-law of BH thermodynamics. In Sec. 5, we first calculate the photon radius by solving the geodesic equation leading to shadow radius. We also estimate the QNMs for this BH solution. Finally, we summarise the results of the paper in the last section.

2 Exact solution of ABG BH with CS

In this section, we construct a new BH solution in the presence of ABG NLED and CS. In this regard, we first write about Einstein's action for the gravity model coupled with ABG NLED and CS as

$$S = \int d^4x \sqrt{-g} [R + \mathcal{L}_{ABG}(F)] + S_{CS}, \quad (1)$$

where g and R are the determinant of metric and curvature scalar respectively. Here, $\mathcal{L}_{ABG}(F)$ refers to Lagrangian density for ABG expressed in terms of invariant $F = \frac{1}{4}F_{\mu\nu}F^{\mu\nu}$, where $F_{\mu\nu} = \nabla_\mu A_\nu - \nabla_\nu A_\mu$ is the Maxwell field-strength tensor, having following form [14, 15, 16, 17]:

$$\mathcal{L}_{ABG}(F) = \frac{F(1 - 3\sqrt{2g^2F})}{(1 + \sqrt{2g^2F})^3} - \frac{3M}{g^3} \left(\frac{(2g^2F)^{5/4}}{(1 + \sqrt{2g^2F})^{5/2}} \right), \quad (2)$$

where parameters M and g are related with the mass and MM charge of the BH, respectively [14, 15]. The electromagnetic field tensor $F_{\mu\nu}$ in 4D spherically spacetime is given by

$$F_{\mu\nu} = 2\delta_{[\mu}^{\theta}\delta_{\nu]}^{\phi}Z(r, \theta) = 2\delta_{[\mu}^{\theta}\delta_{\nu]}^{\phi}g(r)\sin\theta, \quad (3)$$

which leads to $g(r) = g$, where we choose the integration constant as g and it is identified as the MM charge.

$$\frac{1}{4\pi}\int_{s^{\infty}}Fds = \frac{g}{4\pi}\int_0^{\pi}\int_0^{2\pi}\sin\theta d\theta d\phi = g, \quad (4)$$

where s^{∞} is the spherical surface at infinity. Using (4), the field strength tensor can be simplified to

$$F_{\theta\phi} = g\sin\theta, \quad F = \frac{1}{2}\frac{g^2}{r^4}. \quad (5)$$

The explicit expression for the CS action as a source, described by the Nambu-Goto term, is given by [9]

$$S_{\text{CS}} = \int_{\Omega} m\sqrt{-\gamma}d\lambda^0d\lambda^1, \quad (6)$$

where m is the mass of each string, γ is the determinant of $\gamma_{ab} = g_{\mu\nu}\frac{\partial x^{\mu}}{\partial\lambda^a}\frac{\partial x^{\nu}}{\partial\lambda^b}$. $x^{\mu} = x^{\mu}(\lambda^a)$ is describe the string world sheet and $\lambda^a \equiv (\lambda^0, \lambda^1)$, where λ^0 and λ^1 , respectively, are a time-like and space-like coordinates [66]. The $\Omega^{\mu\nu}$ is a bi-vector defined as

$$\Omega^{\mu\nu} = \epsilon^{ab}\frac{\partial x^{\mu}}{\partial\lambda^a}\frac{\partial x^{\nu}}{\partial\lambda^b}, \quad (7)$$

where ϵ^{ab} refers to the two dimensional Levi-Civita tensor defined as $\epsilon^{01} = -\epsilon^{10} = 1$. Furthermore, since $T_{\mu\nu} = 2\partial L/\partial g^{\mu\nu}$, and then $\partial_{\mu}(\sqrt{-g}\rho\Omega^{\mu\nu}) = 0$. Here, ρ is the density, which describes the case of a CS [27], and the $\Omega^{\mu\nu}$ is the function of radial distance. The non-vanishing component of $\Omega^{\mu\nu}$ is $\Omega^{tr} = \Omega^{rt}$. Thus the energy-momentum tensor becomes $T_t^t = T_r^r = -\rho\Omega^{tr}$, and using the $\partial_t(r^2\Omega^{tr}) = 0$ [27]

$$T_t^t = T_r^r = \frac{a}{r^2}, \quad (8)$$

where $a, 0 < a < 1$ is an integration constant related to strings (so-called CS parameter). Varying the action (1) concerning $g_{\mu\nu}$ and A_{μ} , we obtained the following equation of motion (EoM),

$$R_{\mu\nu} - \frac{1}{2}g_{\mu\nu}R = T_{\mu\nu}, \quad (9)$$

$$\nabla_{\mu}\left(\frac{\partial\mathcal{L}_{ABG}(F)}{\partial F}F^{\mu\nu}\right) = 0 \quad \text{and} \quad \nabla_{\mu}(*F^{\mu\nu}) = 0, \quad (10)$$

where the matter energy-momentum tensor (EMT) is given by

$$T_{\mu\nu} = 2\left[\frac{\partial\mathcal{L}_{ABG}(F)}{\partial F}F_{\mu\sigma}F_{\nu}^{\sigma} - g_{\mu\nu}\mathcal{L}_{ABG}(F)\right] + \frac{\rho\Omega_{\mu\sigma}\Omega^{\sigma}_{\nu}}{\sqrt{-\gamma}}, \quad (11)$$

Here, we note that ρ characterises the cloud of strings while m signifies the mass of a single string (for details, see, e.g. [27]). The monopole's topological defects, like cosmic strings and domain walls, originated during the cooling phase of the early universe [67, 68] and play a significant role in investigating BHs. The non-vanishing component of the EMT is

$$T_t^t = T_r^r = \frac{g^2(r^2 - 3g^2)}{(r^2 + g^2)^3} - \frac{6Mg^2}{(r^2 + g^2)^{5/2}} + \frac{a}{r^2}, \quad (12)$$

$$T_{\theta}^{\theta} = T_{\phi}^{\phi} = \frac{g^2(3g^4 - 8g^2r^2 + r^4)}{(g^2 + r^2)^4} + \frac{3g^2M(2g^4 - g^2r^2 - 3r^4)}{(g^2 + r^2)^{9/2}}, \quad (13)$$

where a is a constant identified as the CS parameter. We consider the general static and the spherically symmetric line element to find the BH solution as

$$ds^2 = -f(r)dt^2 + \frac{1}{f(r)}dr^2 + r^2(d\theta^2 + \sin^2\theta d\phi^2), \quad (14)$$

where

$$f(r) = 1 - \frac{2m(r)}{r}. \quad (15)$$

The Einstein field equation is

$$m'(r) = \frac{g^2 r^2 (r^2 - 3g^2)}{2(r^2 + g^2)^3} - \frac{3Mr^2 g^2}{(r^2 + g^2)^{5/2}} + \frac{a}{2}. \quad (16)$$

Integrating Eq. (16) from r to ∞ , we get,

$$-m(r) + \text{Constant} = \int_r^\infty dr \left[\frac{g^2 r^2 (r^2 - 3g^2)}{2(r^2 + g^2)^3} + \frac{3Mr^2 g^2}{(r^2 + g^2)^{5/2}} + \frac{a}{2} \right], \quad (17)$$

and

$$\text{Constant} = \lim_{r \rightarrow \infty} [m(r)] = M. \quad (18)$$

Finally, $m(r)$ is given by

$$m(r) = \frac{Mr^3}{(r^2 + g^2)^{3/2}} - \frac{g^2 r^3}{2(r^2 + g^2)^2} + \frac{a}{2} r, \quad (19)$$

and the solution is given by

$$f(r) = 1 - \frac{2Mr^2}{(r^2 + g^2)^{3/2}} + \frac{g^2 r^2}{(r^2 + g^2)^2} - a. \quad (20)$$

The solution (20) is characterised by BH mass (M), MM charge (g), and CS parameter (a). This exact solution elucidates a new BH solution in the presence of NLED (ABG source) and CS. This solution is a generalised version of the Letelier solution [14, 25] in the absence of MM charge (g), and it interpolates with the ABG BH solution in the absence of CS (a) [40] (when $\alpha = 3, \beta = 4$). this solution (20) resemble with the Schwarzschild BH solution when $a = g = 0$.

Now, let us discuss the horizon structure of the obtained BH solution (20). The horizon radii are zeros of $g^{rr} = 0$ of $f(r_h) = 0$, which implies that

$$1 - \frac{2Mr_h^2}{(r_h^2 + g^2)^{3/2}} + \frac{g^2 r_h^2}{(r_h^2 + g^2)^2} - a = 0, \quad (21)$$

The Eq. (21) cannot be solved analytically, and we need to solve it numerically, and the graphical results are illustrated in Fig. 1. The metric function versus radial coordinate is plotted for various values of the CS parameter (a) and MM charge (g). Such that Eq. (21) admits eight roots (six negative and two positive). The two positive roots r_{\pm} , with r_- and r_+ , represent the Cauchy and event horizons. By keeping the CS parameter (or MM charge) fixed, we find the value of the critical CS parameter (a_c) (or MM charge (g_c)). The Cauchy and event horizons coincide when $r_- = r_+$ corresponds to the extremal BH. The obtained BH solution has two horizon when $a > a_c$ ($g < g_c$) and no horizon when $a < a_c$ ($g > g_c$) (see the table 1 and table 2). Here, one can see that the BH horizon decreases with the growing CS parameter, a , and increases with the growing MM charge, g . The BH horizon coincides at the critical value of MM charge ($g_c = 0.695$) at $a = 0.1$, and the BH horizon is known as the degenerate horizon. For the value of $g > 0.85$, no BH solutions exist. The critical MM charge, g_c , is an increasing function of the CS parameter, a . We have noticed the effect of MM charge and CS parameter are opposite (see Fig. 1).

3 Thermodynamics

In this section, we discuss the thermodynamic properties of the ABG BH with CS. To serve the purpose, let us first calculate the gravitation mass of the BH with the help of the horizon condition ($f(r)|_{r=r_+} = 0$) as

$$M_+ = \frac{1}{\sqrt{r_+^2 + g^2}} \left(\frac{3g^2}{2} - ag^2 + \frac{g^4}{2r_+^2} - \frac{ag^4}{2r_+^2} - \frac{ar_+^2}{2} + \frac{r_+^2}{2} \right). \quad (22)$$

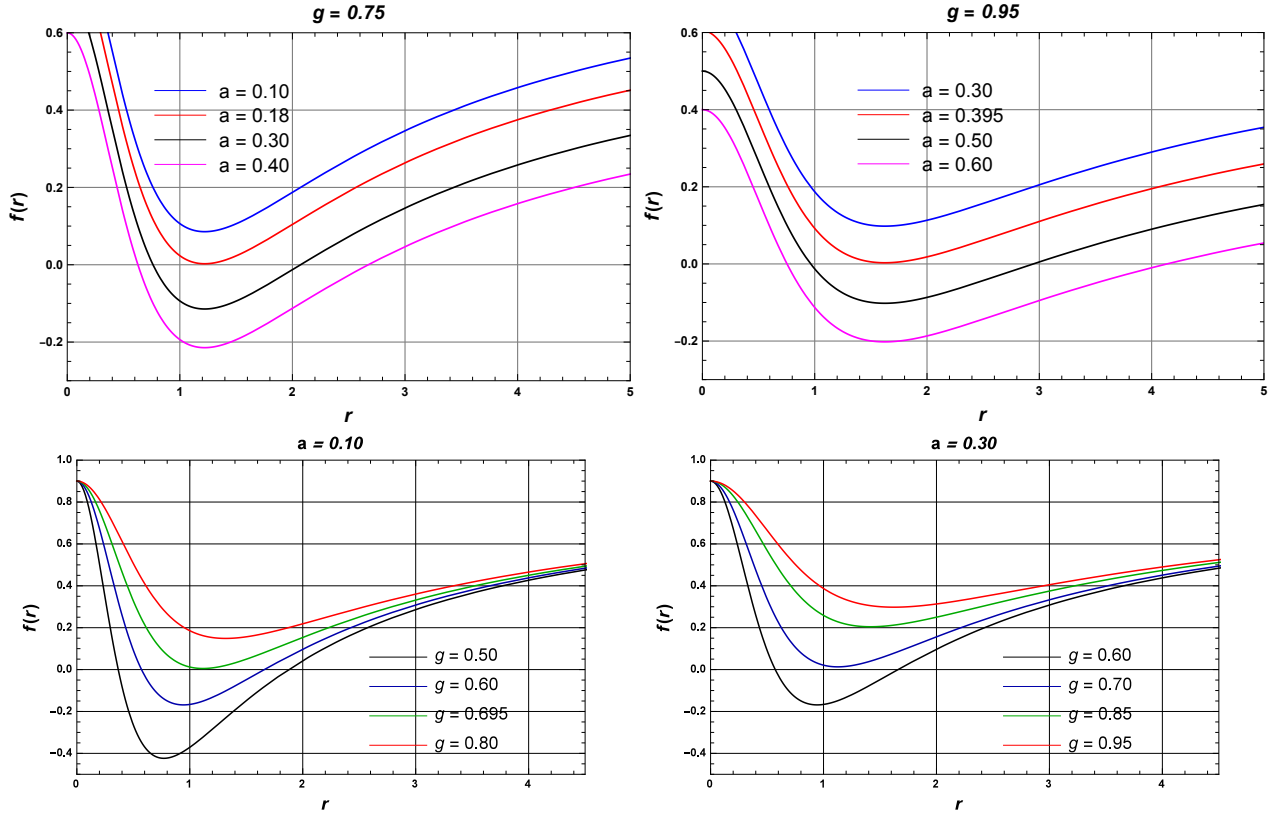


Figure 1: The plot of the metric function $f(r)$ versus r . Upper Panel: For various values of the CS parameter but fixed MM charge ($g = 0.75$ and $g = 0.95$). Lower Panel: For various values of MM charge but fixed CS parameter ($a = 0.1$ and $a = 0.3$) in a unit of M , where $M = 1$.

$g = 0.75$				$g = 0.95$			
a	r_-	r_+	δ	a	r_-	r_+	δ
0.183	1.21	1.21	0	0.395	1.615	1.615	0
0.30	0.761	2.07	1.309	0.50	1.749	1.509	0.240
0.40	0.627	2.67	0.943	0.50	2.945	0.964	0.981

Table 1: The numerical values of inner horizon (r_-), outer horizon (r_+) and $\delta = r_+ - r_-$ for various CS parameter a for $g = 0.75$ and $g = 0.95$ with fixed mass ($M = 1$).

The Hawking temperature is calculated as

$$T_+ = \frac{f'(r)}{4\pi} = \frac{1}{4\pi r_+(r_+^2 + g^2)^3} (r_+^6 - 2g^6 - 3g^4 r_+^2 - g^2 r_+^4 + a(2g^6 + 3g^4 r_+^2 - r_+^6)). \quad (23)$$

The temperature of the obtained BH solution interpolates with the Letelier BH in the limit of $g = 0$ [69]

$$M_+ = \frac{r_+}{2}(1 - a), \quad (24)$$

$$T_+ = \frac{1 - a}{4\pi r_+}. \quad (25)$$

These quantities identify the ABG BH when the CS parameter is switched off [70, 25], i.e.,

$$M_+ = \frac{1}{\sqrt{r_+^2 + g^2}} \left(\frac{3g^2}{2} + \frac{g^2}{2r_+^2} + \frac{r_+^2}{2} \right), \quad (26)$$

$$T_+ = \frac{1}{4\pi r_+(r_+^2 + g^2)^3} (r_+^6 - 2g^6 - 3g^4 r_+^2 - g^2 r_+^4). \quad (27)$$

$a = 0.10$				$a = 0.20$			
g	r_-	r_+	δ	g	r_-	r_+	δ
0.50	0.366	1.875	1.509	0.60	0.432	2.425	0.590
0.60	0.572	1.659	1.087	0.70	0.626	1.216	0.388
0.695	1.11	1.11	0	0.85	1.407	1.407	0

Table 2: Inner horizon (r_-), outer horizon (r_+) and $\delta = r_+ - r_-$ for various MM charge g for $a = 0.10$ and $a = 0.20$ with fixed mass ($M = 1$).

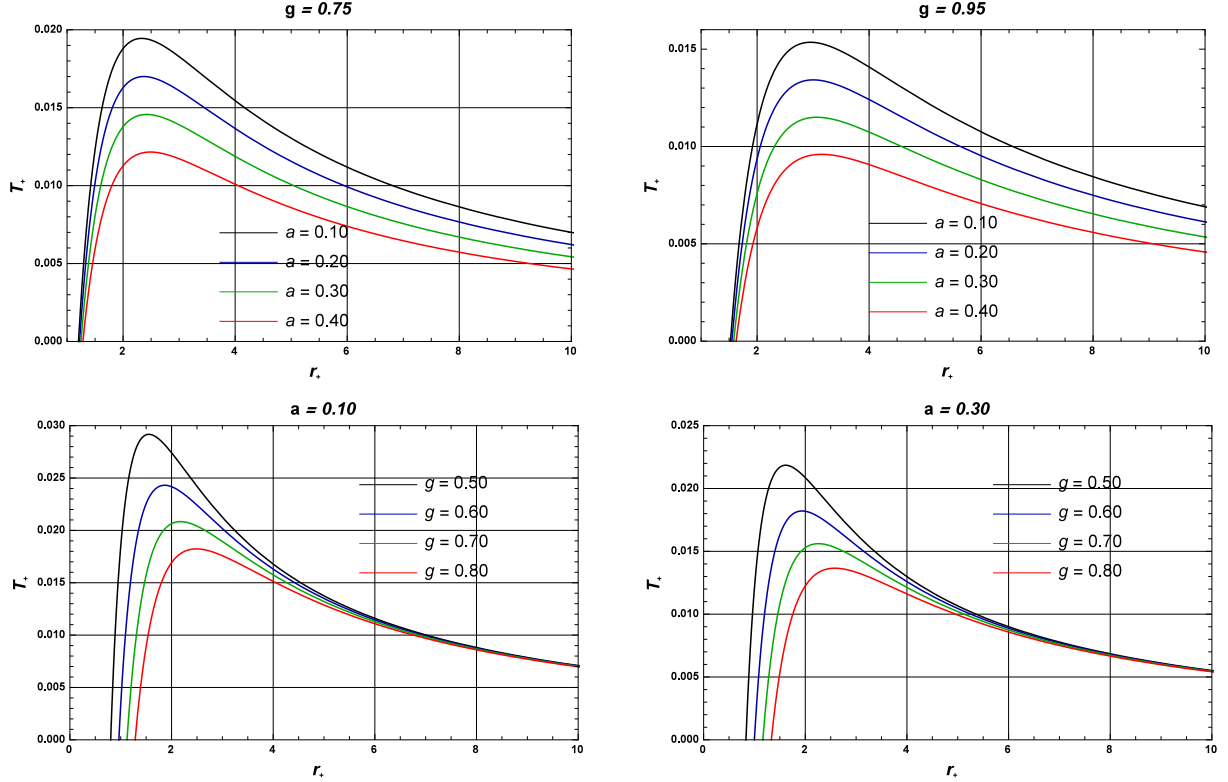


Figure 2: The plot of temperature T_+ vs horizon radius r_+ . Upper Panel: For various CS parameter values with a fixed MM charge value ($g = 0.75$ and $g = 0.95$). Lower Panel: For various values of MM charge with a fixed value of CS parameter ($a = 0.1$ and $a = 0.2$) in the unit of M , where $M = 1$.

However, these quantities coincide with Schwarzschild BH when both the parameters $g = a = 0$.

The entropy of the obtained BH solution can be calculated as this must satisfy the first law of thermodynamics

$$dM_+ = T_+ dS_+ + \Phi dg. \quad (28)$$

At constant charge, the entropy is calculated as

$$S_+ = \int \frac{1}{T_+} \frac{dM_+}{dr_+} dr_+ = \pi r_+ \left(1 - \frac{2g^2}{r_+^2}\right) \sqrt{r_+^2 + g^2} - 3\pi g^2 \ln \left[\sqrt{r_+^2 + g^2} - r_+ \right]. \quad (29)$$

where the terms in bracket of Eq. (29) are due to NLED, which modifies the area law. Here, it is evident that the entropy does not follow the area law. We can also derive the temperature according to the entropy using the first law of thermodynamics

$$T_+ = \frac{\partial M}{\partial S} = \frac{1}{4\pi r_+^4 (r_+^2 + g^2)^{3/2}} \left(r_+^6 - 2g^6 - 3g^4 r_+^2 - g^2 r_+^4 + a(2g^6 + 3g^4 r_+^2 - r_+^6) \right). \quad (30)$$

We have calculated the temperature in Eq. (23) and Eq. (30) of the obtained BH by different methods. The deviation relies on the general structure of the EMT of matter fields. When the BH

mass parameter M is included in the EMT, the conventional form of the first law gets modified with an extra factor [71]

$$\mathcal{C}(M_+, g, r_+) dM_+ = T_+ dS, \quad (31)$$

where T_+ is the Hawking temperature and $\mathcal{C}(M_+, g, r_+)$ is

$$\mathcal{C}(M_+, g, r_+) = 1 + 4\pi \int_{r_+}^{\infty} r_+^2 \frac{\partial T_t^t}{\partial M_+} dr_+ = \frac{r_+^3}{(r_+^2 + g^2)^{3/2}}. \quad (32)$$

We recover the conventional form of the first law of BH thermodynamics when the factor ($\mathcal{C}(M_+, r_+)=1$) because the energy-momentum tensor does not depend upon mass. Because any BH has temperature, it can be seen as a thermodynamic system. Thus, the conventional thermodynamic laws must be satisfied. We have two choices to connect Eq. (31) with the first law of thermodynamics. We know that $\delta E = T_+ \delta S_+$ then the $E \rightarrow M$ and the entropy becomes

$$\delta S_+ = \frac{\mathcal{C}(M_+, g, r_+)}{T_+} \delta M_+, \quad (33)$$

and the the temperature in Eq. (23) and Eq. (30) of the obtained BH solution are same.

Following this modified first law of thermodynamics, the entropy reads

$$S_+ = \pi r_+^2. \quad (34)$$

Now, this entropy agrees with the area law and matches precisely with the entropy of BHs.

4 Local and Global Stability

The heat capacity (C_+) and Gibbs free energy (G_+) study the system's local and global stability. The system is stable when $C_+ > 0$ ($G_+ < 0$) and unstable when $C_+ < 0$ ($G_+ > 0$). The following relation calculates the heat capacity (C_+) of the BH

$$C_+ = \frac{dM_+}{dT_+} = \frac{dM_+}{dr_+} \frac{dr_+}{dT_+}. \quad (35)$$

Substituting the value of the (M_+) from Eq. (22) and (T_+) from Eq. (23) in Eq. (35), we get

$$C_+ = -\frac{2\pi(g^2 + r_+^2)^{5/2}[(1-a)(2g^6 + 3g^4 r_+^2 - r_+^6) + g^2 r_+^4]}{r_+[(1-a)(2g^8 + 11g^6 r_+^2 - r_+^8) + 3(4-5a)g^4 r_+^4 + (8-5a)g^2 r_+^6]}. \quad (36)$$

The heat capacity of the obtained BH solution is plotted in Fig. 3. We observe two kinds of behaviour: first is the positive heat capacity $r < r_c$, suggesting the thermodynamic stability of a BH, and the other is negative heat capacity $r > r_c$, indicating instability of BH. The heat capacity is discontinuous at $r = r_c$, which means that second-order phase transition occurs [72, 73]. It may be noted that the critical radius r_c changes drastically in the presence of the MM charge, and the CS parameter increases. The critical radius rises with the MM charge and CS parameter increase.

The following relation calculates the Gibbs free energy (G_+) of the BH:

$$G_+ = M_+ - T_+ S_+. \quad (37)$$

Substituting the value of the (M_+) from Eq. (22) and (T_+) from Eq. (23) in Eq. (37), we get

$$G_+ = \frac{(1-a)(r_+^2 + g^2) + r_+^2 g^2 (3-2a)}{2r_+^2 \sqrt{g^2 + r_+^2}} + \frac{r_+[(1-a)(2g^6 + 2g^4 r_+^2 - r_+^6) + g^2 r_+^4]}{4(g^2 + r_+^2)^3}. \quad (38)$$

Interestingly, the discontinuity of the heat capacity occurs at $r = 1.6$ for $g = 0.60$ and $a = 0.10$, at which point the Hawking temperature reaches the maximum value, and the Gibbs free energy reaches the minimum value. Hence, the phase transition occurs from the lower to higher mass, corresponding to a black hole's positive to negative heat capacity.

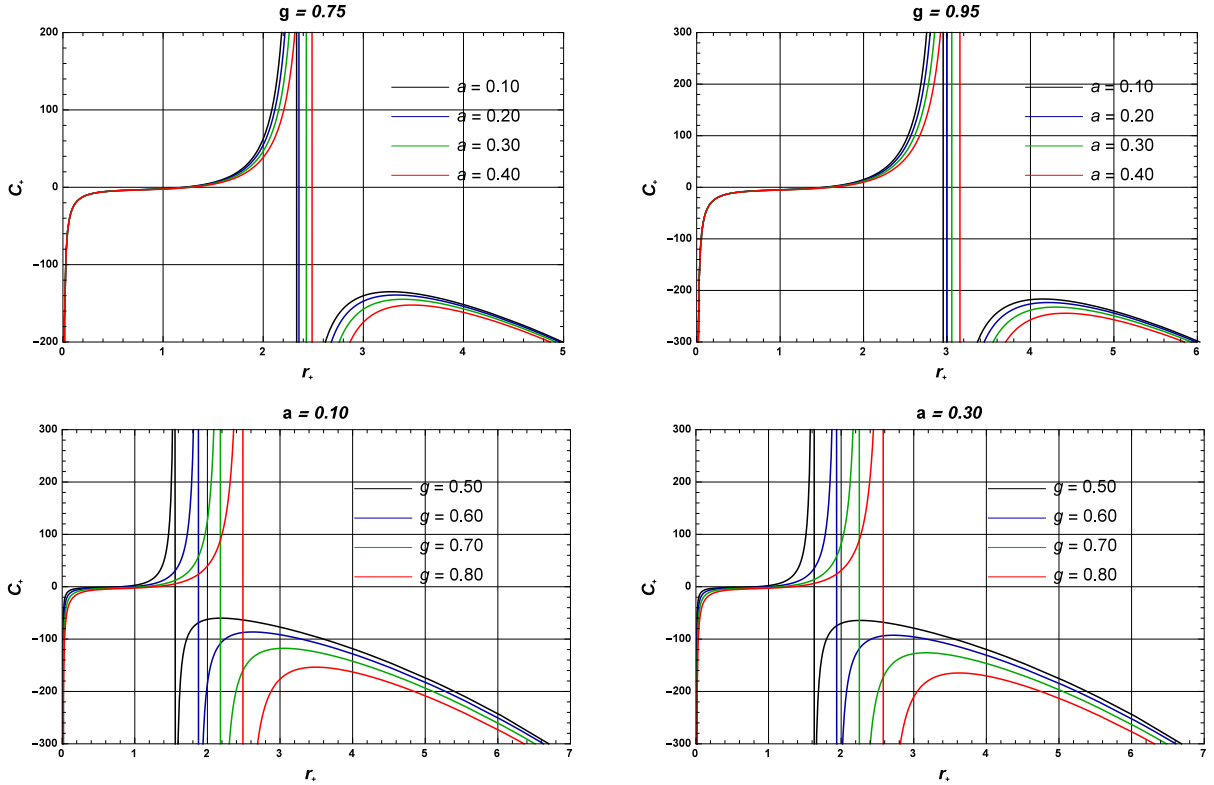


Figure 3: The plot of heat capacity C_+ vs horizon radius r_+ . Upper Panel: For various values of CS parameter with a fixed value of MM charge ($g = 0.75$) and ($g = 0.95$). Lower Panel: For various values of MM charge with a fixed value of CS parameter ($a = 0.1$) and ($a = 0.3$).

The BH remnant is a well-merited entity in theoretical astrophysics that can be a source of dark energy [74] and is one of the candidates to resolve the information loss puzzle [75]. The double root $r = r_e$ of $f(r) = 0$ corresponds to the extremal BH with a degenerate horizon. Hence $f'(r) = 0$, and the critical radius is

$$r_e = \frac{g}{(1-a)} \sqrt{\left(\frac{1}{3} - \frac{22^{1/3} g^2}{A} \left[\frac{5}{3} + \frac{3a^2}{2} - 3a \right] - \frac{A}{32^{1/3}} \right)}, \quad (39)$$

where

$$A = 3M^2 \left(2g^{12} + 27g^8 M^4 - 54g^6 M^6 + 3\sqrt{3} \sqrt{-8g^{18} M^6 - 9g^{16} M^8 - 108g^{14} M^{10}} \right)^{1/3}, \quad (40)$$

and the corresponding mass is

$$M_e = \frac{1}{\sqrt{r_e^2 + g^2}} \left(\frac{g^2(3-2a)}{2} + \frac{(g^4 + r_e^4)(1-a)}{2r_e^2} \right). \quad (41)$$

It can be seen from (23) that the temperature decreases with increasing r_+ and vanishes when the two horizons coincide $T_+ \rightarrow 0, C_+ \rightarrow 0$.

5 Shadow and Quasinormal Modes

In this section, we study the shadow and quasinormal modes of the BH solution coupled with ABG NLED and CS. We begin by assuming that a photon is moving around the BH. The photon is restricted to move in the equatorial plane (i.e. $\theta = \pi/2$). The Hamiltonian that leads to the equation of motion [76, 77, 78],

$$H = \frac{1}{2} \left[-\frac{p_t^2}{f(r)} + f(r)p_r^2 + \frac{p_\phi^2}{r^2} \right]. \quad (42)$$

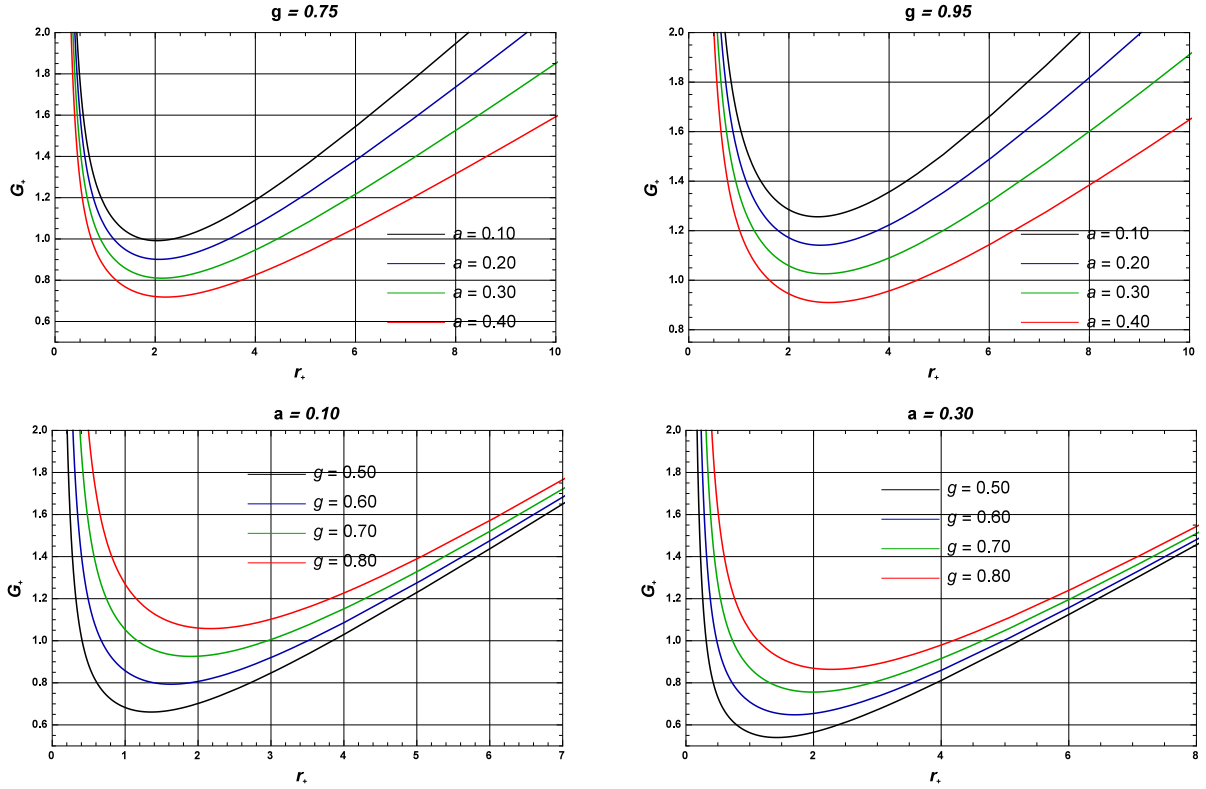


Figure 4: The plot of heat capacity C_+ vs horizon radius r_+ . Upper Panel: For various values of CS parameter with a fixed value of MM charge ($g = 0.75$) and ($g = 0.95$). Lower Panel: For various values of MM charge with a fixed value of CS parameter ($a = 0.1$) and ($a = 0.3$).

The canonically conjugate momenta corresponding to the line element (14) with metric function (20) are

$$p_t = \left(1 - \frac{2Mr^2}{(r^2 + g^2)^{3/2}} + \frac{g^2 r^2}{(r^2 + g^2)^2} - a \right) \dot{t} = \mathcal{E}, \quad (43)$$

$$p_r = \left[\left(1 - \frac{2Mr^2}{(r^2 + g^2)^{3/2}} + \frac{g^2 r^2}{(r^2 + g^2)^2} - a \right) \right]^{-1} \dot{r}, \quad (44)$$

$$p_\theta = r^2 \dot{\theta}, \quad \text{and} \quad p_\phi = r^2 \sin^2 \theta \dot{\phi} = L. \quad (45)$$

Here, \mathcal{E} and L represent the energy and angular momentum of the photon, respectively.

By exploiting the equations of motion and conserved quantities, the radial null circular geodesics reads

$$\dot{r}^2 + V_{eff}(r) = 0 \quad \text{where} \quad V_{eff} = f(r) \left(\frac{L^2}{r^2} + \frac{\mathcal{E}^2}{f(r)} \right). \quad (46)$$

For null circular geodesics, V_{eff} must satisfy the following conditions:

$$V_{eff} = 0, \quad \frac{\partial V_{eff}}{\partial r} = 0, \quad (47)$$

which lead to

$$3Mr^4(r^2 + g^2) - \sqrt{r^2 + g^2}(2g^2 r^4 + (1 - a)(g^2 + r^2)^3) = 0. \quad (48)$$

The solution of this equation gives photon radius. However, this equation is not solvable analytically; therefore, this can be solved numerically. The numerical photon radius values for different MM charges and CS parameter values are appended in table 3. From the list, we notice that the effects of the CS parameter, a , and MM charge, g , on photon radii are in contrast. The photon radius increases when the CS parameter increases, a , but decreases when the MM charge, g , increases.

a	r_p								
	$g = 0.1$	$g = 0.2$	$g = 0.3$	$g = 0.4$	$g = 0.5$	$g = 0.6$	$g = 0.7$	$g = 0.8$	$g = 0.9$
0.1	3.319	3.736	4.273	4.988	5.989	7.489	9.990	14.991	29.992
0.2	3.275	3.695	4.235	4.952	5.956	7.459	9.963	14.966	29.970
0.3	3.200	3.625	4.170	4.892	5.900	7.408	9.916	14.924	29.932
0.4	3.080	3.522	4.075	4.805	5.821	7.336	9.851	14.865	29.879
0.5	2.928	3.379	3.945	4.688	5.715	7.241	9.765	14.788	29.727
0.6	2.697	3.181	3.773	4.536	5.580	7.121	9.658	14.693	29.811
0.7	2.318	2.897	3.541	4.340	5.411	6.973	9.529	14.580	29.628
0.8	...	2.386	3.211	4.084	5.200	6.794	9.374	14.446	29.512
0.9	2.582	3.729	4.933	6.577	9.193	14.293	29.379

Table 3: The numerical values of photon radius with different values of a and g in unit of M , where $M = 1$.

5.1 Black Hole Shadow

With the help of photon radius, we can now compute the shadow of a BH (20). The BH shadow radius (r_s) depends on photon sphere radius as [79]

$$r_s = \frac{r}{\sqrt{f(r)}} \Big|_{r=r_p}. \quad (49)$$

The numerical values of the shadow radius are given in table 4 and plotted in Fig. 5 for various BH parameters. Here, it is evident that the shadow radius increases along with the increasing CS parameter, a , but decreases with the increasing MM charge, g .

a	r_s								
	$g = 0.1$	$g = 0.2$	$g = 0.3$	$g = 0.4$	$g = 0.5$	$g = 0.6$	$g = 0.7$	$g = 0.8$	$g = 0.9$
0.1	6.068	6.015	5.924	5.789	5.600	5.338	4.945
0.2	7.244	7.191	7.100	6.967	6.785	6.540	6.203	5.680	...
0.3	8.854	8.801	8.710	8.578	8.400	8.166	7.860	7.445	6.794
0.4	11.162	11.108	11.016	10.884	10.707	10.480	10.192	9.825	9.341
0.5	14.678	14.623	14.529	14.325	14.218	13.993	13.714	13.371	12.946
0.6	20.520	20.462	20.365	20.227	20.045	19.818	19.540	19.206	18.806
0.7	31.602	31.540	31.436	31.289	31.098	30.860	30.573	30.233	29.835
0.8	58.071	58.001	57.884	57.720	57.506	57.243	56.928	56.559	56.133
0.9	164.28	164.19	164.04	163.83	163.56	163.22	162.82	162.36	161.83

Table 4: The numerical values of shadow radius for different values of CS parameters (a) and MM charge (g) in a unit of M , where $M = 1$.

5.2 QNMs of Black Hole Solution

In this subsection, we utilise the scalar QNMs of the BH to investigate the dynamical stability of the solution, and this is characterised by the real and imaginary parts of the complex QNM frequencies (QNFs), $\omega = \omega_R + i\omega_I$. The condition $\omega > 0$ confirms that the BH is unstable, and condition $\omega < 0$ indicates that the BH is stable. We consider scalar field perturbations of the BH solution. The QNMs and QNFs can be computed from the solution of the following scalar field equation for the BH background:

$$\frac{1}{\sqrt{-g}} \partial_\mu (\sqrt{-g} g^{\mu\nu} \partial_\nu) \psi = 0. \quad (50)$$

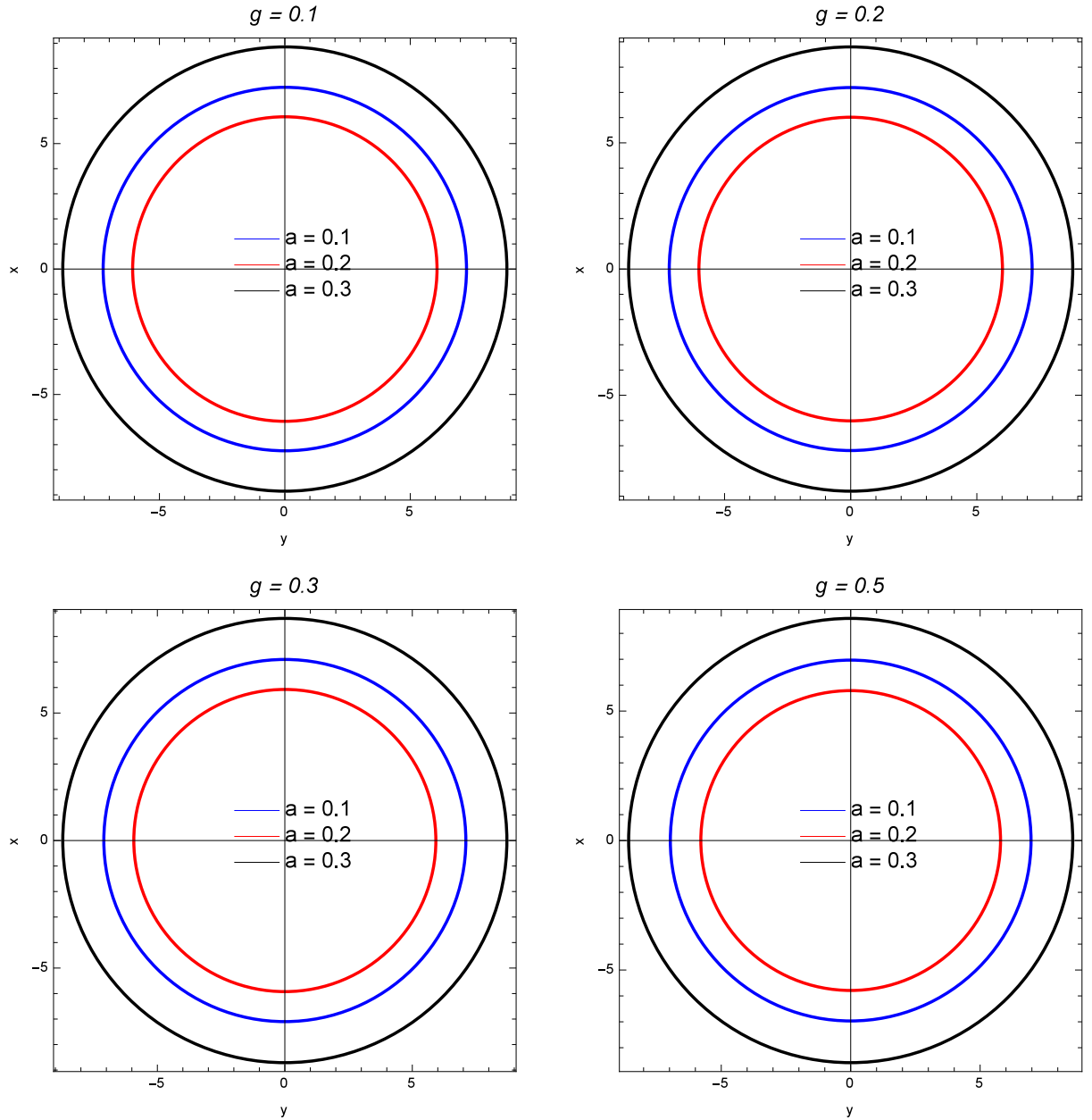


Figure 5: The BH shadow for different CS parameter (a) and MM charge (g).

This equation can be solved by separating the variables as,

$$\psi = \frac{1}{r} \sum_{lm} e^{i\omega t} u_{lm}(r) Y_l^m(\theta, \phi), \quad (51)$$

where Y_l^m are spherical harmonics. For the tortoise coordinate $dr^* = dr/f(r)$, the radial part of the solution takes the Schrödinger-like form

$$\left(\frac{d^2}{dr^{*2}} + \omega^2 - V_0(r^*) \right) u(r) = 0, \quad (52)$$

where, $V_0(r^*) = f(r) \left(\frac{f'(r)}{f(r)} + \frac{l(l+1)}{r^2} \right)$. We use the WKB method to solve the QNFs in large l limit [80, 81, 82, 83] as

$$\omega = l\Omega - i \left(n + \frac{1}{2} \right) |\Lambda|, \quad (53)$$

with

$$\Omega = \frac{\sqrt{f(r_p)}}{r_p} = \frac{1}{L_p} \quad \text{and} \quad \Lambda = \frac{\sqrt{2f(r_p) - r_p^2 f''(r_p)}}{\sqrt{2}L_p}. \quad (54)$$

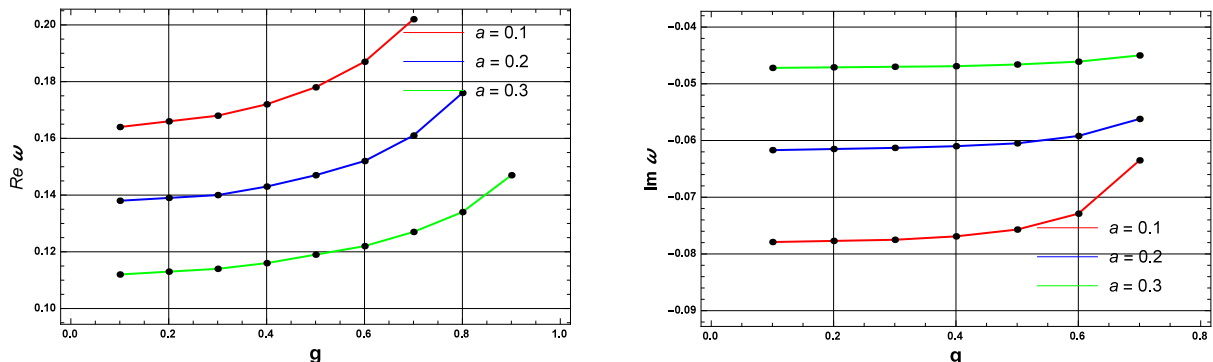


Figure 6: Left panel: The real part of QNFs for various values of MM charge (g) with fixed M . Right panel: The imaginary part of QNFs for various values of MM charge (g) in a unit of M , where $M = 1$.

The numerical values of QNFs are tabulated in tables 5 and 6 and plotted in Fig. 6 for the different BH parameters.

a	ω_R								
	$g = 0.1$	$g = 0.2$	$g = 0.3$	$g = 0.4$	$g = 0.5$	$g = 0.6$	$g = 0.7$	$g = 0.8$	$g = 0.9$
0.1	0.164	0.166	0.168	0.172	0.178	0.187	0.202
0.2	0.138	0.139	0.140	0.143	0.147	0.152	0.161	0.176	...
0.3	0.112	0.113	0.114	0.116	0.119	0.122	0.127	0.134	0.147
0.4	0.0895	0.0900	0.0907	0.0918	0.0933	0.0954	0.0981	0.101	0.107
0.5	0.0681	0.0683	0.0688	0.0694	0.0703	0.0714	0.0729	0.0747	0.0722
0.6	0.0487	0.488	0.0491	0.0494	0.0498	0.0504	0.0511	0.0520	0.0531
0.7	0.0316	0.0317	0.0318	0.0319	0.0321	0.0324	0.0327	0.0330	0.0335
0.8	0.0172	0.0172	0.0172	0.0173	0.0173	0.0174	0.0175	0.0176	0.0178
0.9	0.006	0.006	0.006	0.006	0.006	0.006	0.006	0.006	0.006

Table 5: The numerical values of the real part of QNMs for various CS parameters, a and MM charge, g in a unit of M . Here, $M = 1$, $l = 1$ and $n = 0$.

The behaviour of QNMs and QNFs under the influence of parameters a and g are depicted in Fig. 6. Here, the fundamental part of the QNMs decreases with a and increases with the g while the imaginary part increases (almost constant) with g . The negative imaginary part of the QNFs confirms the stable modes of the obtained BH solution; However, at the large MM charge, the obtained BH solution is unstable.

6 Results and Conclusions

In this work, we have constructed a new exact BH solution when the gravity is minimally coupled to ABG NLED and CS source. We have considered the ABG NLED term, which characterises the MM charge. The horizon structure of the obtained BH solution is explored. The size of the BH decreases with an increase in MM charge, g , and increases with the CS parameter, a . The thermodynamics of BHs is also studied. Here, we have found that this BH solution follows the modified first law of thermodynamics, which leads to entropy that follows the area law.

a	$-\omega_I$								
	$g = 0.1$	$g = 0.2$	$g = 0.3$	$g = 0.4$	$g = 0.5$	$g = 0.6$	$g = 0.7$	$g = 0.8$	$g = 0.9$
0.1	0.077	0.0777	0.0775	0.0769	0.0757	0.0729	0.0635
0.2	0.061	0.0615	0.0613	0.0610	0.0605	0.0592	0.0562	0.0439	...
0.3	0.047	0.0471	0.0470	0.0469	0.0466	0.0461	0.0450	0.0423	0.0300
0.4	0.034	0.0346	0.0346	0.0345	0.0344	0.0342	0.0338	0.0331	0.0312
0.5	0.024	0.0240	0.0240	0.0240	0.0240	0.0239	0.0238	0.0236	0.0232
0.6	0.015	0.153	0.0154	0.0154	0.0153	0.0153	0.0153	0.0153	0.0152
0.7	0.008	0.0086	0.0086	0.0086	0.0086	0.0086	0.0086	0.0086	0.0086
0.8	0.003	0.0038	0.0038	0.0038	0.0038	0.0038	0.0038	0.0038	0.0038
0.9	0.0009	0.0009	0.0009	0.0009	0.0009	0.0009	0.0009	0.0009	0.0009

Table 6: The numerical values of the imaginary part of QNMs for different CS parameters, a and MM charge, g in a unit of M . Here, $M = 1$, $l = 1$ and $n = 0$.

We numerically calculated the photon sphere radii and QNMs, including the shadow of the obtained BH solution. We have found that the MM charge and CS parameter affect the photon radius and shadow radius. In particular, the photon sphere radius and shadow radius increase with the CS parameter but decrease with the MM charge. It will be attractive to investigate the effects of thermal fluctuation on the thermodynamics of this BH.

Data Availability Statement

Data sharing does not apply to this article as no data sets were generated or analysed during the current study.

Acknowledgement

DVS thanks the DST-SERB project (grant no. EEQ/2022/000824) and IUCAA, Pune, for the hospitality while this work was being done.

References

- [1] B. P. Abbott et al. (LIGO Scientific, Virgo), Phys. Rev. Lett. 116, 061102 (2016).
- [2] K. Akiyama et al. (Event Horizon Telescope), Astrophys. J. Lett. 875, L1-L6 (2019).
- [3] K. Akiyama et al. (Event Horizon Telescope), Astrophys. J. Lett. 930, L12 (2022).
- [4] M. Born and L. Infeld, Proc. R. Soc. Lond. 144, 425 (1934).
- [5] N. Seiberg and E. Witten, J. High Energy Phys. 09, 032 (1999).
- [6] P. Paul, S. Upadhyay and D. V. Singh, Eur. Phys. J. Plus 138, 566 (2023).
- [7] Y. Myrzakulov, K. Myrzakulov, S. Upadhyay and D. V. Singh, Int. J. Geom. Meth. Mod. Phys. 20, 2350121 (2023); K. Esmakhanova, Y. Myrzakulov, G. Nugmanova and R. Myrzakulov, Int. J. Theor. Phys. 51, 1204 (2012).
- [8] B. Pourhassan, M. Dehghani, S. Upadhyay, I. Sakalli and D. V. Singh, Mod. Phys. Lett. A 37, 2250230 (2022).
- [9] D. V. Singh, A. Shukla and S. Upadhyay, Annals of Physics 447, 169157 (2022).
- [10] V. A. De Lorenci, R. Klippert, M. Novello and J. M. Salim, Phys. Rev. D 65, 063501 (2002).

- [11] M. Novello, S. E. P. Bergliaffa and J. Salim, *Phys. Rev. D* 69, 127301 (2004).
- [12] R. P. Mignani et al., *Mon. Not. R. Astron. Soc.* 465, 492 (2016).
- [13] E. S. Fradkin and A. A. Tseytlin, *Phys. Lett. B* 163, 123 (1985).
- [14] E. Ayón-Beato and A. García, *Phys. Rev. Lett.* 80, 5056 (1998).
- [15] E. Ayón-Beato and A. García, *Phys. Lett. B* 464, 25 (1999).
- [16] E. Ayón-Beato and A. García, *Phys. Lett. B* 493, 149 (2000).
- [17] E. Ayón-Beato and A. García, *Gen. Rel. Grav.* 37, 635 (2005).
- [18] D. V. Singh, S. G. Ghosh and S. D. Maharaj, *Nucl. Phys. B* 981, 115854 (2022).
- [19] D. V. Singh and N. K. Singh, *Annals Phys.* 383, 600 (2017).
- [20] A. A. A. Filho, *Class. Quant. Grav.* 41, 015003 (2024).
- [21] A. Biswas, *Gen. Rel. Grav.* 54, 161 (2022).
- [22] R. Kumar Walia, S. G. Ghosh and S. D. Maharaj, *Astrophys. J.* 939, 77 (2022).
- [23] A. Belhaj and Y. Sekhmani, *Eur. Phys. J. Plus* 137, 278 (2022).
- [24] A. Kumar, D. V. Singh, Y. Myrzakulov, G. Yergaliyeva and S. Upadhyay, *Eur. Phys. J. Plus* 138, 1071 (2023).
- [25] P. S. Letelier, *Phys. Rev. D* 28, 2414 (1983).
- [26] P. S. Letelier, *Il Nuovo Cim. B* 63, 519 (1981).
- [27] P.S. Letelier, *Phys. Rev. D* 20, 1294 (1979).
- [28] D. V. Singh, S. G. Ghosh and S. D. Maharaj, *Phys. Dark Univ.* 30, 100730 (2020).
- [29] R. Takahashi and J. Korean Phys. Soc. 45, S1808 (2004).
- [30] P. V. P. Cunha, C. A. R. Herdeiro and M. J. Rodriguez, *Phys. Rev. D* 97, 084020 (2018).
- [31] B. K. Vishvakarma, D. V. Singh and S. Siwach, *Phys. Scripta* 99, 025022 (2024).
- [32] B. K. Vishvakarma, D. V. Singh and S. Siwach, *Eur. Phys. J. Plus* 138, 536 (2023).
- [33] M. Zubair, M. A. Raza, F. Sarikulov and J. Rayimbaev, *JCAP* 10, 058 (2023).
- [34] S. Mandal, S. Upadhyay, Y. Myrzakulov, G. Yergaliyeva, *Int. J. Mod. Phys. A* 38, 2350047 (2023).
- [35] S. Upadhyay, S. Mandal, Y. Myrzakulov, and K. Myrzakulov, *Annals of Physics* 450, 169242 (2023).
- [36] D. V. Singh, V. K. Bhardwaj, S. Upadhyay, *Eur. Phys. J. Plus* 137, 969 (2022).
- [37] J. Jing, Q. Pan, *Phys. Lett. B* 660, 13 (2008) .
- [38] S. Chandrasekhar, S. Detweller, *Proc. R. Soc. Lond. Ser. A Math. Phys. Eng. Sci.* 344, 441 (1975).
- [39] P.-Hui Mou, Y.-Xian Chen, K.-Jian He and G.-Ping Li, *Commun. Theor. Phys.* 74, 125401 (2022).
- [40] X. C. Cai and Y. G. Miao, *Phys. Rev. D* 103, 124050 (2021).

- [41] D. J. Gogoi, R. Karmakar and U. D. Goswami, *Int. J. Geom. Meth. Mod. Phys.* 20, 2350007 (2023).
- [42] M. Murshid, F. Rahaman and M. Kalam, *Indian J. Phys.* 97, 295 (2023).
- [43] R. A. Konoplya, D. Ovchinnikov and B. Ahmedov, *Phys. Rev. D* 108, 104054 (2023).
- [44] D. J. Gogoi, J. Bora, M. Koussour and Y. Sekhmani, *Annals Phys.* 458, 169447 (2023).
- [45] K. Jafarzade, M. Kord Zangeneh and F. S. N. Lobo, *Annals Phys.* 446, 169126 (2022).
- [46] J. M. Ladino and E. Larrañaga, *Int. J. Theor. Phys.* 62, 209 (2023).
- [47] P.-C. Li, T.-C. Lee, M. Guo, and B. Chen, *Phys. Rev. D* 104, 084044 (2021).
- [48] K. Jusufi, *Phys. Rev. D* 101, 124063 (2020).
- [49] J. D. Bekenstein, *Lett. Nuovo Cim.* 4, 737 (1972).
- [50] J. D. Bekenstein, *Phys. Rev. D* 7, 2333 (1973).
- [51] S. W. Hawking, *Phys. Rev. D* 13, 191 (1976).
- [52] A. Strominger and C. Vafa, *Phys. Lett. B* 379, 99 (1996).
- [53] S. Carlip, *Phys. Rev. Lett.* 82, 2828 (1999).
- [54] S. Upadhyay, *Phys. Lett. B* 775, 130 (2017).
- [55] S. Upadhyay, B. Pourhassan and H. Farahani, *Phys. Rev. D* 95, 106014 (2017).
- [56] S. Upadhyay, N.-ul-Islam, P. A. Ganai, *JHAP* 2, 25 (2022).
- [57] B. Pourhassan, H. Farahani, F. Kazemian, Izzet Sakalli, S. Upadhyay, D. V. Singh, *Physics of the Dark Universe* 44, 101444 (2024).
- [58] B. Pourhassan, S. Upadhyay, H. Saadat and H. Farahani, *Nucl. Phys. B* 928, 415 (2018).
- [59] S. Upadhyay, *Gen. Rel. Grav.* 50, 128 (2018).
- [60] S. Chougule, S. Upadhyay, H. K. Sudhanshu and S. Kumar, *JHAP* 3, 45 (2023).
- [61] S. S. Shahraeini, K. Nozari and S. Saghafi, *JHAP* 2, 55 (2022).
- [62] S. Soroushfar, B. Pourhassan and I. Sakalli, *Physics of the Dark Universe* 44, 101457 (2024).
- [63] B. Pourhassan, I. Sakalli, X. Shi, M. Faizal and S. S. Wani, *EPL* 144, 29001 (2023).
- [64] B. Pourhassan and I. Sakalli, *Chinese Journal of Physics* 79, 322 (2022).
- [65] M. Yasir, T. Xia and S. Upadhyay, *Phys. Scr.* 99, 065003 (2024).
- [66] J. L. Synge, *Relativity: The General Theory*, p. 175v, (North Holland, Amsterdam, 1966).
- [67] M. Barriola and A. Vilenkin, *Phys. Rev. Lett.* 63, 341 (1989).
- [68] T. W. B. Kibble, *J. Phys. A* 9, 1387 (1976).
- [69] S. G. Ghosh, U. Papnoi and S. D. Maharaj, *Phys. Rev. D* 90, 044068 (2014).
- [70] B. K. Singh, R. P. Singh and D. V. Singh, *Eur. Phys. J. Plus* 136, 575 (2021).
- [71] M.-Sen Ma and R. Zhao, *Class. Quant. Grav.* 31, 245014 (2014).
- [72] S. G. Ghosh, D. V. Singh and S. D. Maharaj, *Phys. Rev. D* 97, 104050 (2018).

- [73] S. W. Hawking and D. N. Page, *Commun. Math. Phys.* 87, 577 (1983).
- [74] J. H. MacGibbon, *Nature (London)* 329, 308 (1987).
- [75] J. Preskill, arXiv: hep-th/9209058.
- [76] A. Belhaj, H. Belmahi, M. Benali, W. El Hadri, H. El Moumni and E. Torrente-Lujan, *Phys. Lett. B* 812, 136025 (2021) .
- [77] A. Belhaj and Y. Sekhmani, *Gen. Rel. Grav.* 54, 17 (2022).
- [78] A. Belhaj, H. Belmahi, M. Benali and A. Segui, *Phys. Lett. B* 817, 136313 (2021).
- [79] V. Perlick, O. Y. Tsupko and G. S. Bisnovatyi-Kogan, *Phys. Rev. D* 92, 104031 (2015).
- [80] B. F. Schutz and C. M. Will, *Astrophys J.* 291, L33 (1985).
- [81] S. Iyer and C. M. Will, *Phys. Rev. D* 35, 3621(1987).
- [82] R. A. Konoplya, *Phys. Rev. D* 68, 024018 (2003).
- [83] V. Cardoso, A. S. Miranda, E. Berti, H. Witek and V. T. Zanchin, *Phys. Rev. D* 79, 064016 (2009).

A Ricci curvature invariants

The Ricci scalar (R) is given by

$$\begin{aligned}
R &= \frac{2a}{r^2} - \frac{24g^2r^2}{(r^2 + g^2)^4} + \frac{30Mr^4}{(r^2 + g^2)^{7/2}} + \frac{36g^2r^2}{(r^2 + g^2)^3} - \frac{54Mr^2}{(r^2 + g^2)^{5/2}} - \frac{12g^2}{(r^2 + g^2)^2} \\
&+ \frac{24M}{(r^2 + g^2)^{3/2}}.
\end{aligned} \tag{55}$$

Without the CS parameter and MM charge, the Ricci scalar (55) is zero.

The Ricci square ($R_{\mu\nu}R^{\mu\nu}$) is given by

$$\begin{aligned}
R_{\mu\nu}R^{\mu\nu} &= \frac{2a^2}{r^4} + \frac{288g^4r^8}{(r^2 + g^2)^8} - \frac{720g^2Mr^8}{(r^2 + g^2)^{15/2}} - \frac{672g^4r^6}{(r^2 + g^2)^7} + \frac{450M^2r^8}{(r^2 + g^2)^7} + \frac{1848g^2Mr^6}{(r^2 + g^2)^{13/2}} \\
&+ \frac{568g^4r^4}{(r^2 + g^2)^6} + \frac{1260M^2r^6}{(r^2 + g^2)^6} - \frac{1740g^2Mr^4}{(r^2 + g^2)^{11/2}} - \frac{216g^4r^2}{(r^2 + g^2)^5} + \frac{1314M^2r^4}{(r^2 + g^2)^5} + \frac{756g^2Mr^2}{(r^2 + g^2)^{9/2}} \\
&+ \frac{36g^4}{(r^2 + g^2)^4} - \frac{648M^2r^2}{(r^2 + g^2)^2} - \frac{144g^2M}{(r^2 + g^2)^{7/2}} + \frac{16ag^2}{(r^2 + g^2)^3} + \frac{144M^2}{(r^2 + g^2)^3} + \frac{144M^2}{(r^2 + g^2)^3} \\
&- \frac{24aM}{(r^2 + g^2)^{5/2}} - \frac{12ag^2}{r^2(r^2 + g^2)^2} + \frac{24aM}{r^2(r^2 + g^2)^{3/2}}.
\end{aligned} \tag{56}$$

Without the CS parameter and MM charge, the Ricci scalar (56) is zero.

The Kretschmann scalar ($R_{\mu\nu\lambda\sigma}R^{\mu\nu\lambda\sigma}$) is calculated by

$$\begin{aligned}
R_{\mu\nu\lambda\sigma}R^{\mu\nu\lambda\sigma} &= \frac{4a^2}{r^4} + \frac{576g^4r^8}{(r^2 + g^2)^8} - \frac{1440g^2Mr^8}{(r^2 + g^2)^{15/2}} - \frac{960g^4r^6}{(r^2 + g^2)^7} + \frac{900M^2r^8}{(r^2 + g^2)^7} \\
&+ \frac{2640g^2Mr^6}{(r^2 + g^2)^{13/2}} + \frac{560g^4r^4}{(r^2 + g^2)^6} + \frac{1800M^2r^6}{(r^2 + g^2)^6} - \frac{1704g^2Mr^4}{(r^2 + g^2)^{11/2}} - \frac{144g^4r^2}{(r^2 + g^2)^5} \\
&+ \frac{1284M^2r^4}{(r^2 + g^2)^5} + \frac{504g^2Mr^2}{(r^2 + g^2)^{9/2}} + \frac{24g^4}{(r^2 + g^2)^4} - \frac{432M^2r^2}{(r^2 + g^2)^2} - \frac{96g^2M}{(r^2 + g^2)^{7/2}} \\
&+ \frac{96M^2}{(r^2 + g^2)^3} - \frac{8ag^2}{r^2(r^2 + g^2)^2} + \frac{16aM}{r^2(r^2 + g^2)^{3/2}}.
\end{aligned} \tag{57}$$

The Kretschmann scalars ($R_{\mu\nu\lambda\sigma}R^{\mu\nu\lambda\sigma}$) (57) reduces to $48M^2/r^6$ in the limit of $a = g = 0$. These invariants diverge in the limit of $r \rightarrow 0$ and, thus, signify a singular black hole solution. In the absence of a CS parameter, these invariants become singular.